Molecular Genetics and Metabolism 141 (2024) 108149

Contents lists available at ScienceDirect

Molecular Genetics and Metabolism

journal homepage: www.elsevier.com/locate/ymgme

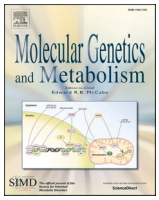

PCYT2 deficiency in Saarlooswolfdogs with progressive retinal, central, and peripheral neurodegeneration

Matthias Christen [a], Anna Oevermann [b], Stefan Rupp [c], Frédéric M. Vaz [d,e,f], Eric J.M. Wever [d,e,f,g], Barbara K. Braus [h], Vidhya Jagannathan [a], Alexandra Kehl [i,j], Marjo K. Hytönen [k,l,m], Hannes Lohi [k,l,m], Tosso Leeb [a,*]

[a] Institute of Genetics, Vetsuisse Faculty, University of Bern, Bern 3001, Switzerland
[b] Division of Neurological Sciences, Vetsuisse Faculty, University of Bern, Bern 3001, Switzerland
[c] Neurology Department, Tierklinik Hofheim, IVC Evidensia, Hofheim am Taunus 65719, Germany
[d] Amsterdam UMC, University of Amsterdam, Department of Clinical Chemistry and Pediatrics, Laboratory Genetic Metabolic Diseases, Emma Children's Hospital, Meibergdreef 9, Amsterdam, the Netherlands
[e] Amsterdam Gastroenterology Endocrinology Metabolism, Inborn Errors of Metabolism, Amsterdam, the Netherlands
[f] Core Facility Metabolomics, Amsterdam UMC, University of Amsterdam, Amsterdam, the Netherlands
[g] Bioinformatics Laboratory, Department of Epidemiology & Data Science, Amsterdam Public Health Research Institute, University of Amsterdam, 1100 DE Amsterdam UMC, the Netherlands
[h] Ophthalmology Department, Tierklinik Hofheim, IVC Evidensia, Hofheim am Taunus 65719, Germany
[i] Laboklin GmbH & Co. KG, Steubenstraße 4, Bad Kissingen 97688, Germany
[j] Comparative Experimental Pathology, School of Medicine, Technical University of Munich (TUM), Munich, Germany
[k] Department of Medical and Clinical Genetics, University of Helsinki, Helsinki 00014, Finland
[l] Department of Veterinary Biosciences, University of Helsinki, Helsinki 00014, Finland
[m] Folkhälsan Research Center, Helsinki 00290, Finland

ARTICLE INFO

Keywords:
Canis lupus familiaris
Neurology
Ophthalmology
Kennedy pathway
Inborn error of metabolism
Precision medicine
Animal model

ABSTRACT

We investigated a syndromic disease comprising blindness and neurodegeneration in 11 Saarlooswolfdogs. Clinical signs involved early adult onset retinal degeneration and adult-onset neurological deficits including gait abnormalities, hind limb weakness, tremors, ataxia, cognitive decline and behavioral changes such as aggression towards the owner. Histopathology in one affected dog demonstrated cataract, retinal degeneration, central and peripheral axonal degeneration, and severe astroglial hypertrophy and hyperplasia in the central nervous system. Pedigrees indicated autosomal recessive inheritance. We mapped the suspected genetic defect to a 15 Mb critical interval by combined linkage and autozygosity analysis. Whole genome sequencing revealed a private homozygous missense variant, *PCYT2*:c.4A>G, predicted to change the second amino acid of the encoded ethanolamine-phosphate cytidylyltransferase 2, XP_038402224.1:(p.Ile2Val). Genotyping of additional Saarlooswolfdogs confirmed the homozygous genotype in all eleven affected dogs and demonstrated an allele frequency of 9.9% in the population. This experiment also identified three additional homozygous mutant young dogs without overt clinical signs. Subsequent examination of one of these dogs revealed early-stage progressive retinal atrophy (PRA) and expansion of subarachnoid CSF spaces in MRI. Dogs homozygous for the pathogenic variant showed ether lipid accumulation, confirming a functional PCYT2 deficiency. The clinical and metabolic phenotype in affected dogs shows some parallels with human patients, in whom *PCYT2* variants lead to a rare form of spastic paraplegia or axonal motor and sensory polyneuropathy. Our results demonstrate that *PCYT2*:c.4A>G in dogs cause PCYT2 deficiency. This canine model with histopathologically documented retinal, central, and peripheral neurodegeneration further deepens the knowledge of PCYT2 deficiency.

Abbreviations: CDP, cytidine diphosphate; CSF, cerebrospinal fluid; CTP, cytidine triphosphate; ECVO, European College of Veterinary Ophthalmologists; HPLC, high-performance liquid chromatography; MRI, magnetic resonance imaging; OMIA, Online Mendelian Inheritance in Animals; OMIM, Online Mendelian Inheritance in Man; PC, phosphatidylcholine; PCR, polymerase chain reaction; PCYT2, ethanolamine-phosphate cytidylyltransferase 2; PE, phosphatidylethanolamine; PRA, progressive retinal atrophy; PS, phosphatidylserine; SNV, single nucleotide variant.

* Corresponding author.
E-mail address: tosso.leeb@unibe.ch (T. Leeb).

https://doi.org/10.1016/j.ymgme.2024.108149
Received 19 December 2023; Received in revised form 19 January 2024; Accepted 19 January 2024
Available online 21 January 2024

1. Introduction

Phosphatidylethanolamines (PE) comprise around 15–25% of phospholipids in mammalian cell membranes and are the second most common type of phospholipids after phosphatidylcholines (PC) [1,2]. The multitude of different PE functions encompasses stabilization of membrane anchored proteins, promotion of membrane fusion and fission, conformational changes in protein structure, protein integration into membranes and many more [3–5]. PE are particularly enriched in nervous tissues, such as the white matter of the brain or the retina, where they can account for up to 45% of all phospholipids [1].

Synthesis of PE is regulated by two main pathways in eukaryotic cells. During phosphatidylserine (PS) decarboxylation, PS is transported into the mitochondria and subsequently decarboxylated to form the majority of mitochondrial PE [6,7]. On the other hand, the CDP-ethanolamine pathway as part of the so-called Kennedy pathway is the only way for *de novo* synthesis of PE but also of corresponding ether lipids (PE-O) [8–10]. PE and PE-O synthesis is carried out in three enzymatic steps, during which ethanolamine and diacylglycerol or alkyl-acyl glycerol are converted to PE and PE-O, respectively. During the second and rate-limiting synthesis step, the formation of CDP-ethanolamine out of CTP and phosphoethanolamine is catalyzed by the phosphate cytidylyltransferase 2 (PCYT2), which is encoded by the *PCYT2* gene [11,12]. In the last step, CDP-ethanolamine condenses with diacylglycerol or 1-alkyl-2-acylglycerol to form PE and PE-O, respectively.

Biallelic variants in *PCYT2* have been described as the cause of spastic paraplegia 82 (SPG82, OMIM #618770) in a total of eleven human patients [13–18], and additionally in two siblings with axonal motor and sensory polyneuropathy [19]. Individuals with PCYT2 deficiency display a broad spectrum of neurological symptoms including ataxia, spasticity, seizures, and visual impairment [19]. *Pcyt2*$^{-/-}$ null mice are not viable and embryos die after implantation, while *Pcyt2*$^{+/-}$ mice display alterations in hepatic fatty acid composition and develop key features of metabolic syndrome [20,21]. Additionally, muscle specific Pcyt2 deficiency leads to impaired muscle- and whole-body growth in mice [22].

This study was prompted by reports of Saarlooswolfdogs with blindness that was in most cases confirmed to be the consequence of progressive retinal atrophy (PRA), in combination with subsequently emerging gradually worsening neurological deficits that included weakness, ataxia, and behavioral changes. We hypothesized that the dogs might be affected by an inherited disease and initiated sample collection for a genetic study. After identification of a candidate causative variant and genotyping of a large cohort of dogs, additional clinical, pathological and metabolic investigations of affected dogs were performed.

2. Material and methods

2.1. Ethics statement

All examinations and animal experiments were done after obtaining owner's consent and in accordance with local laws, regulations, and ethical guidelines. Blood samples were collected with the approval of the Cantonal Committee for Animal Experiments (Canton of Bern; permits BE 71/19 and BE94/2022) and the animal ethical committee of the County Administrative Board of Southern Finland (ESAVI/6054/04.10.03/2012, ESAVI/343/04.10.07/2016 and ESAVI/25696/2020).

2.2. Animal selection for genetic analysis

The Saarlooswolfdog breed originated from a cross between a German Shepherd dog and an Eurasian grey wolf (*Canis lupus lupus*) in the Netherlands in 1932. The breed was officially recognized by FCI in 1975. This study was conducted with samples of 1091 Saarlooswolfdogs from three different biobanks. A total of 783 samples came from the Vetsuisse Biobank and included 156 samples that had been collected >20 years ago at the Ruhr University Bochum. Based on the available phenotype information, each dog was assigned to one of six gross categories: 'healthy' ($n = 542$), 'neurologic' ($n = 19$), 'ophthalmologic' ($n = 60$), 'combined neurologic and ophthalmologic' ($n = 14$), 'disease phenotype, other' ($n = 11$), or 'no phenotype information' ($n = 137$). Reports of ophthalmologic exams by board certified veterinary ophthalmologists (ECVO) were used to determine ocular phenotypes when available. All other phenotype information was initially based on owner reports. Further information and refined classification according to age at investigation and ECVO status can be found in supplementary Table S1.

An additional 157 samples were provided by the University of Helsinki Dog DNA biobank and 151 samples were provided by Laboklin in Germany. These samples all came from Saarlooswolfdogs without reports of combined neurologic and ophthalmologic phenotypes and were classified as controls. Names and available registration numbers of dogs of the three cohorts were compared to ensure that there was no overlap.

2.3. Detailed phenotypic classification

Breeders and owners reported 14 dogs that we classified as 'combined neurologic and ophthalmologic'. After subjective review of the owner-reported phenotypes, we sub-grouped these dogs into 11 dogs that exhibited a specific combination of blindness/PRA together with an adult-onset neurodegeneration involving ataxia, hind limb weakness and behavioral changes. These dogs are subsequently referred to as cases 1–11. The remaining three other 'combined neurologic and ophthalmologic' dogs showed non progressive epileptic episodes that responded well to medication. Their ophthalmologic phenotype was isolated cataract without suspicion of retinal degeneration. We therefore hypothesized that these two subgroups might have shown two distinct phenotypes, rather than signs of one single disease.

During the course of the study, we identified three young dogs that were clinically healthy, but carried the same homozygous mutant *PCYT2* genotype as cases 1–11. These three dogs are subsequently termed Homozygous Young (HY)1–3. HY1 and HY2 came from the same litter and were 17 months old at the time of writing, whereas HY3 was 33 months old.

2.4. Histopathological investigation

During the investigations, case 9 was euthanized because of progressing neurological signs and the body of the dog was donated for histopathological investigation. Selected tissues included eye bulbs, central nervous system, peripheral nerves, skeletal muscle, heart muscle, intestine, liver, skin, and eyelid. Samples were immersion-fixed in 4% neutral buffered formaldehyde, embedded in paraffin, sectioned at 4 μm, and stained with hematoxylin and eosin (HE). Selected brain and spinal cord sections were histochemically stained with combined Luxol fast blue-HE, Masson-Trichrome stain or modified Bielschowsky stain, or were immunohistochemically assessed for glial fibrillary acidic protein (GFAP) expression.

2.5. DNA extraction and SNV genotyping

Genomic DNA was extracted from EDTA blood using the Maxwell RSC Whole Blood DNA kit in combination with the Maxwell RSX instrument (Promega, Dübendorf, Switzerland) and a semi-automated Chemagen extraction robot (PerkinElmer Chemagen Technologie, Waltham, MA, USA).

DNA from 16 dogs was genotyped on illumina_HD canine BeadChips containing 220,853 markers (Neogen, Lincoln, NE, USA). Eight dogs were affected by neurodegeneration and progressive loss of vision (cases 1, 2, 3, 4, 6, 7, 10, and 11), and eight were control dogs. Two of the

Table 1
Ophthalmologic phenotypes of 11 Saarlooswolfdogs with blindness and neurodegeneration.

Case no.	Ophthalmologic phenotype[a]	Age at diagnosis
1	owner-reported blindness, no ophthalmological examination	n.a.
2	PRA + zero response in electroretinogram, report not available	3y[b]
3	owner-reported blindness, no ophthalmological examination	n.a.
4	PRA + ectopic cilia	3y 10 m
5	PRA + cataract + glaucoma, report not available	–
6	PRA (no date on examination report)	–
7	PRA	3y 9 m
8	PRA	4y 10 m
9	PRA + cataract	4y 10 m
10	PRA	1y 7 m
11	PRA + cataract	1y 8 m

[a] If not stated otherwise, reports of ophthalmological exams were available to confirm the diagnoses.
[b] blind since age of 3 years, but unknown, whether the examination was done at the same time.

affected dogs (cases 10 and 11), as well as all control dogs (sire, dam, and six healthy offspring) belonged to one single family. The raw SNV genotypes are available in the supplementary File S1.

2.6. Linkage analysis and homozygosity mapping

For all dogs, the call rate was >95%. For linkage analysis, markers that were missing, non-informative, on sex chromosomes, and had Mendel errors or a minor allele-frequency <0.05 were removed using PLINK v1.9 [23]. The final pruned dataset contained 72,698 markers. They were then analyzed for parametric linkage using an autosomal recessive inheritance model with full penetrance and a disease allele frequency of 0.3 together with the Merlin software [24].

The genotype data of eight affected dogs were used for homozygosity mapping. Markers that were missing in one of the cases and markers on the sex chromosomes were excluded. The –homozyg and –homozyg-group options in PLINK were used to search for extended regions of homozygosity >1 Mb. The output intervals were visually matched against the linked intervals in Excel spreadsheets to find overlapping regions. All positions correspond to the UU_Cfam_GSD_1.0 reference genome assembly.

2.7. Whole genome resequencing

An Illumina TruSeq PCR-free library with ~380 bp insert size was prepared from case 6. We collected 210 million 2 × 150 bp paired end reads on a NovaSeq 6000 instrument (23.5× coverage). Mapping to the UU_Cfam_GSD_1.0 reference genome assembly was performed as described [25]. The sequence data were deposited under study accession PRJEB16012 and sample accession SAMEA8157188 at the European Nucleotide Archive.

2.8. Variant calling and filtering

Variant calling was performed using the GATK HaplotypeCaller [26] in gVCF mode as described [25]. To filter for private variants in the affected dogs, we used genome sequences from 1495 control dogs of diverse breeds (Table S2) [25,27]. The 1495 controls dogs did not contain any Saarlooswolfdogs. The predicted functional effects of the called variants were annotated with SnpEff software [28] together with the UU_Cfam_GSD_1.0 reference genome assembly and NCBI annotation release 106.

2.9. PCR and Sanger sequencing

The candidate variant, *PCYT2*:XM_038546296.1:c.4A>G, was genotyped by direct Sanger sequencing of PCR amplicons. A 346 bp PCR product was amplified with primers 5'-GCC AGG TGC GCG TGC GCT AT-3' and 5'-CTC ACC AGC CGT CGC ACC ACA C-3′ using AmpliTaqGold360MasterMix (Thermo Fisher Scientific, Waltham, MA, USA) with the addition of 20% 360 GC Enhancer (Thermo Fisher Scientific) in the reaction volume. After an initial denaturation step for 10 min at 95 °C, 35 cycles of 30 s denaturation at 95 °C, 30 s annealing at 68 °C, and 1 min of polymerization at 72 °C followed. After a final extension step of 7 min at 72 °C, the samples were cooled to 4 °C for storage. Quality control of the PCR reaction was performed using a 5200 Fragment Analyzer (Agilent, Santa Clara, CA, USA). Samples were then treated with exonuclease I and alkaline phosphatase and subsequently sequenced with ABI BigDye v3.1 (Thermo Fisher Scientific). The sequencing reactions were purified using ethanol precipitation and analyzed on an ABI 3730 DNA Analyzer (Thermo Fisher Scientific) and the raw sequence data were analyzed with Sequencher 5.1 software (GeneCodes, Ann Arbor, MI, USA).

2.10. Clinical characterization of HY1

A clinical, neurological, and ophthalmological examination was performed, which was impeded by aggressive behaviour of the dog. Anaesthesia was induced with propofol (Narcofol, CP-Pharma, Burgdorf, Germany) and after endotracheal intubation maintained with inhalation of isoflurane (Isoflurane CP, CP-Pharma, Burgdorf, Germany). An MRI of the brain (Vantage Elan, Canon medial Systems, Germany) and an electroretinogram (RETIport, Roland Consult, Brandenburg, Germany) were performed under general anaesthesia.

2.11. Lipidomics analysis

Plasma was extracted from thawed EDTA blood samples of 18 Saarlooswolfdogs (six per *PCYT2*:c.4 A>G genotype) and used for lipidomics analysis. Samples from dogs with the homozygous mutant *G/G* genotype were from cases 4, 6, 7, 9, 11, and from HY2. All samples from homozygous wildtype and heterozygous dogs came from the group "Healthy, with ECVO certificate, >5 years at investigation". The lipidomics analysis was performed as previously described [29,30].

3. Results

3.1. Pedigree analyses and phenotype classification

This project was initiated by reports from breeders indicating that several suspected genetic disorders may be segregating in the Saarlooswolfdog breed. We carefully reviewed the available reports by owners and breeders and finally identified eleven dogs that shared a combination of blindness due to retinal degeneration and signs of a neurodegenerative disease. These eleven affected dogs had an even sex distribution comprising five males and six females and were born between 1999 and 2019. They belonged to seven distantly related litters, four of them with two affected puppies each and three in litters with no other affected dogs. All parents were reportedly healthy. All affected puppies were inbred to a common ancestor within 4–10 generations.

PRA diagnosis was made by an ophthalmologist in 9/11 cases. Additional ocular phenotypes were reported in four cases (Table 1). In the six dogs with known examination date, the PRA diagnosis was made between 20 and 46 months of age (av: 36 m, SD: 17 m). For cases 1 and 3, owners reported progressive loss of vision, but retinal atrophy was not objectified by a veterinarian.

The eleven affected dogs additionally exhibited a range of neurological and neuromuscular signs, including gait abnormalities, hind limb weakness, tremors, ataxia, cognitive decline and behavioral changes

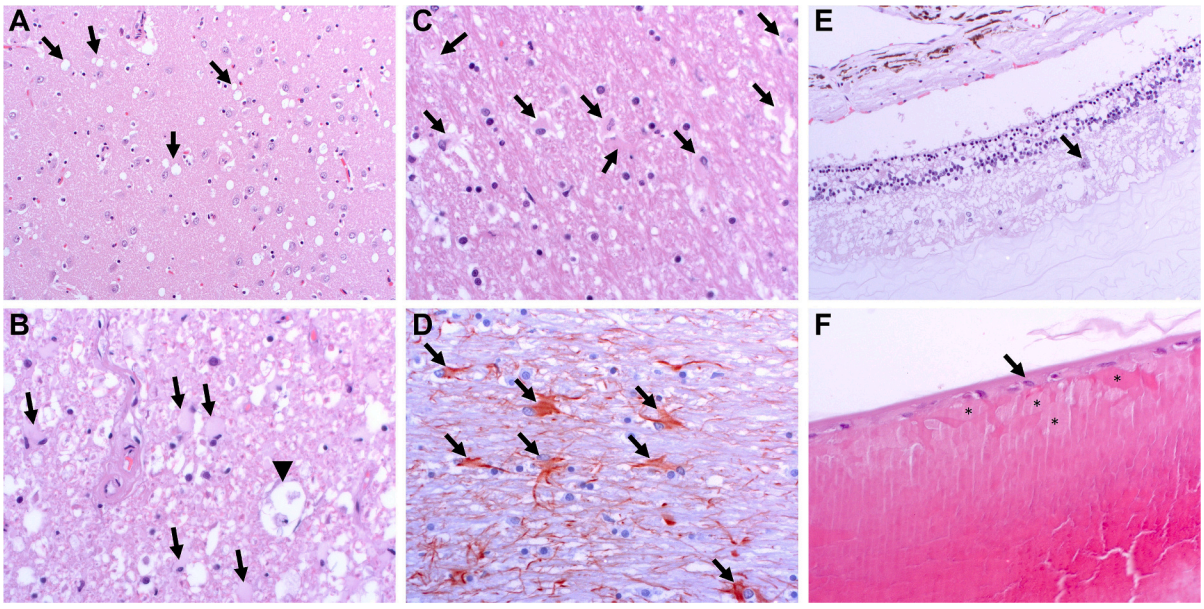

Fig. 1. Histopathological features of case 9. A. Caudate nucleus shows numerous well-defined clear vacuoles of variable size (arrows). HE stain, 100× magnification. B. The dorsal funiculi of the spinal cord contain numerous hypertrophic astrocytes with large cytoplasm (arrows) and dilated myelin sheaths with myelinophages and fragmented axons (arrowhead). HE stain, 400× magnification. C. The cerebellar white matter contains numerous hypertrophic astrocytes with large irregular to lobulated nuclei (arrows). HE stain, 400× magnification. D. Immunohistochemistry for GFAP shows large hypertrophic astrocytes with thick cellular processes (arrows). 400× magnification. E. The retina is atrophic and has lost its layered structure. The outer and inner nuclear layers are fused. Retinal ganglion cells are strongly reduced in numbers. The arrow highlights a remnant ganglion cell. HE stain, 200× magnification. F. The caudal pole of the lens shows posterior migration of lens epithelium (arrow) and presence of subcapsular Morgagnian globules.

Table 2
Results of variant filtering in an affected dog against 1495 control genomes.

Filtering step	Homozygous variants
all variants in the affected dog	2,519,081
private variants in whole genome	34,296
protein-changing private variants in whole genome	106
private variants in the critical interval	1000
protein-changing private variants in the critical interval	16
in functional candidate genes for similar phenotypes in other species	1

Table 3
Association of the *PCYT2*:c.4A>G variant with the phenotype in 1091 Saarlooswolfdogs.

Phenotype group[a]	*A/A*	*A/G*	*G/G*
healthy (n = 542)	429	110	3
neurologic (n = 19)	18	1	–
ophthalmologic (n = 60)	49	11	–
combined neurologic and ophthalmologic (*n* = 14)[b]	1	2	11
disease phenotype, other (n = 11)	9	2	–
no phenotype information (n = 137)	115	22	–
control dogs Helsinki (*n* = 157)	127	30	–
control dogs Laboklin (*n* = 151)	124	27	–

[a] For details of the phenotype classes, see Methods, section 2.2.
[b] The 3 discordant dogs had epilepsy and cataract, but no signs of retinal degeneration.

such as aggression towards the owner. Videos of gait abnormalities in cases 4 and 9 are available in supplementary video S1. Additionally, epileptic seizures were reported in cases 5, 6, 8, and 11. MRI was reportedly done at four years of age in cases 7, 9 and 10. The MRIs of cases 7 and 10 showed brain atrophy compatible with neurodegenerative disease. Notably, MRI findings in case 9 were normal even though it was performed after the onset of neurological signs. A detailed compilation of the available diagnostic reports in the affected dogs is listed in supplementary Table S3.

Age of death for seven affected dogs was between 26 and 119 months of age (av: 69 m, SD: 31 m), compared to an average life expectancy of 12.5 years in the breed. Case 3 was euthanized because of blindness; the other six cases were euthanized because of the progression of the neurological signs and impaired quality of life. Cases 5, 7, 8 and 10 were still alive at time of writing, with 10, 6, 6 and 4 years of age, respectively.

3.2. Histopathological investigation case 9

Histopathology of case 9, euthanized at 63 months of age, revealed severe bilateral retinal degeneration with loss of layering and atrophy. The outer and inner nuclear layers were thin and partially fused, and the outer plexiform layer and the rod/cone layer were barely visible (Fig. 1). The inner plexiform layer was loose, and the number of ganglion cells was severely reduced. Additionally, there was bilateral cataract with presence of capsular epithelium (posterior migration of lens epithelium) and Morgagnian globules at the caudal poles.

Brain and spinal cord showed scattered hypertrophy and hyperplasia of white matter astrocytes, which had a large amount of cytoplasm and large irregular to lobulated nuclei. These changes were most prominent in the spinal cord, brainstem, cerebellar medulla and in the corona radiata. Multiple small glial nodules were present in the white matter of the spinal cord and brainstem. The cerebellar foliae appeared slightly thin with widening of the sulci. Gliosis was observed in the molecular layer, and Purkinje cells appeared to be irregularly distributed. The neuropil of the caudate nucleus, and to a lesser extent the cortex, contained well-defined vacuoles of variable sizes that were associated with astrocytic hypertrophy.

In addition to the astrocytic hypertrophy, axonal swelling/degeneration and dilation of myelin sheaths containing axonal fragments were observed in the spinal cord. The changes were most severe in the dorsal funiculi, and particularly in the cervical spinal cord. However, milder changes were also found in other funiculi. The cuneate and gracile

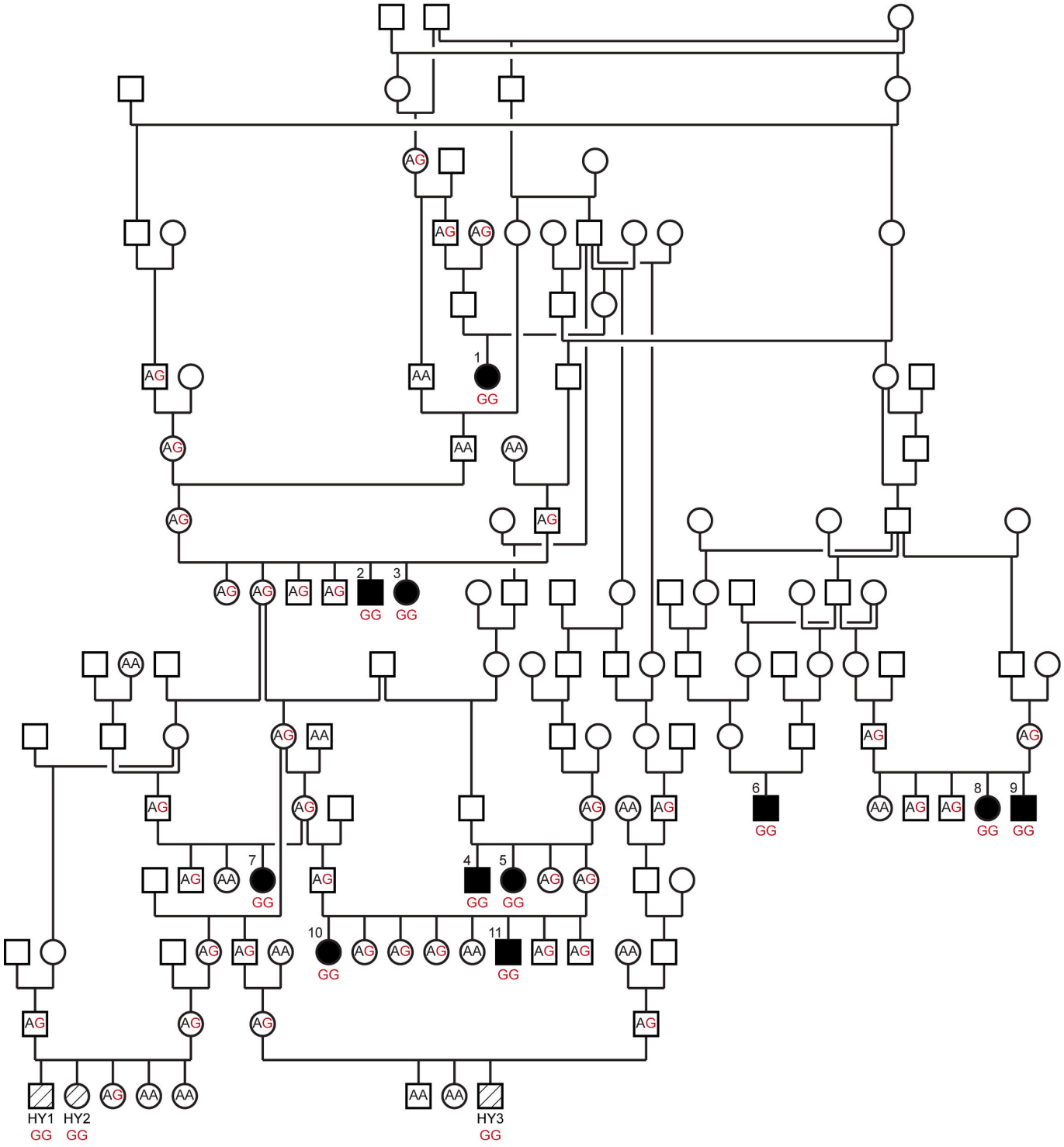

Fig. 2. Pedigree of Saarlooswolfdogs and co-segregation of the genotypes at the *PCYT2*:c.4A>G variant with the disease. Cases 1–11 are numbered and indicated with filled symbols. The three additional homozygous mutant, but clinically healthy dogs HY1–3 are indicated with striped symbols. Squares represent males, circles females. Genotypes at the *PCYT2*:c.4A>G variant are indicated for all dogs, from which a DNA sample was available. Typical for purebred dogs, all affected dogs are inbred and share common ancestors on the paternal and maternal side. The pedigree is suggestive for a monogenic autosomal recessive inheritance of the trait.

nucleus in the brainstem contained multiple axonal spheroids. Myelin ballooning was observed multifocally in the dorsal root ganglia, with multiple axons being swollen, pale, and surrounded by a very thin myelin sheet. Multifocal mild meningothelial proliferation was additionally observed in the subarachnoid space of spinal cord and cerebellum.

Skeletal muscles multifocally contained single myofibers or myofiber groups that were atrophic and triangular to flat in appearance, with multifocal internalization of nuclei. Multiple terminal nerve fibers showed increased interstitial fibrosis that separated the axons.

3.3. Genetic analysis

We hypothesized a monogenic autosomal recessive mode of

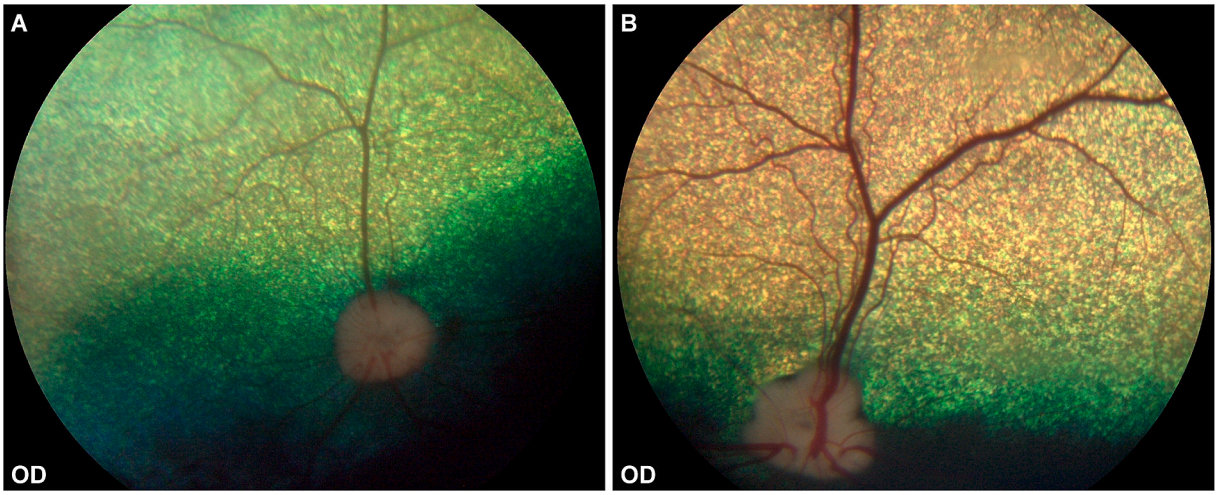

Fig. 3. Retinal changes. A. Fundus image of the right eye (OD) of the investigated dog HY1, illustrating the vascular attenuation and tapetal hyperreflectivity. B. Fundus image of a healthy control dog for comparison.

inheritance as multiple dogs from the same litters with reportedly healthy parents were affected by a highly similar combination of PRA and neurological deficits. Parametric linkage analysis in one family consisting of the parents and eight offspring identified 29 linked segments spanning 214 Mb with a maximum LOD score of 1.35. Homozygosity mapping in eight affected dogs identified eight extended homozygous regions with shared haplotypes. A total of two genomic segments on chromosomes 3 and 9 showed simultaneous linkage in the family and homozygosity in the eight cases. Taken together, these two intervals spanned 15.2 Mb or 0.64% of the 2.4 Gb dog genome and were considered the critical interval for the subsequent analyses (Table S4).

The genome of case 6 was sequenced and searched for homozygous private protein changing variants by comparing the variants to 1495 control genomes (Table 2, Table S5). Further prioritization of resulting variants was then done according to functional knowledge of affected genes.

The bioinformatics analysis identified one single homozygous private protein-changing variant in a functional candidate gene within the critical interval. The variant, chr9:1,207,490A>G or XM_038546296.1:c.4A>G, was located in the *PCYT2* gene and is predicted to result in an amino acid substitution in the encoded ethanolamine-phosphate cytidylyltransferase 2, XP_038402224.1:(p.Ile2Val). The other 15 private protein-changing variants within the critical interval were not located in genes known to cause similar combined ocular and neurologic phenotypes in humans, mice, or domestic animals.

The variant was genotyped in a cohort of 1091 Saarlooswolfdogs (Table 3). All eleven investigated cases carried a homozygous mutant *G/G* genotype at the *PCYT2* variant. The frequency of the mutant allele in 998 dogs without reports of neurologic or ophthalmologic phenotypes was 9.9%. The frequency of heterozygous carriers in this cohort was 19.1%. The genotype distribution in this cohort significantly deviated from Hardy-Weinberg equilibrium with only 3 instead of 9.7 expected homozygous mutant dogs ($p = 0.017$).

The three homozygous mutant dogs in the healthy cohort were all younger than the average age for PRA diagnosis in this study (<36 m), and clinically still normal. These healthy young dogs were termed HY1–3. HY1 was subsequently clinically examined to investigate a potential early *PCYT2*-related phenotype (see below, section 3.4).

Genotypes at the variant co-segregated with the observed phenotype in the pedigree, and all fourteen homozygous dogs shared a common ancestor on the paternal and maternal side, as would be expected for a monogenic autosomal recessive mode of inheritance (Fig. 2).

3.4. Clinical investigation of HY1

Dog HY1 was examined at 9 months of age. General clinical and neurological examinations could not be fully completed, as the dog showed aggression towards the examiner. The available examinations remained without special findings.

Ophthalmic examination was performed under general anaesthesia due to aggression. Both eyes were quiet, normotensive, the corneal health unremarkable and the lens clear. Fundic examination revealed mild bilateral tapetal hyperreflectivity. This was more pronounced above the tapetal/non tapetal border as a subtle hyperreflective horizontal line. Additional findings were mild-moderate vascular attenuation and optic nerve pallor (Fig. 3A).

Electroretinography carried out in the right eye revealed absent rod function, a reduced mixed rod-cone response (1.3 Hz), and an unremarkable cone flicker (28 Hz). The overall ophthalmologic findings were consistent with generalized progressive retinal atrophy, most likely progressive rod cone degeneration (prcd-PRA).

MRI of the head showed minimal expansion of the subarachnoid CSF spaces, which can represent a normal variation, but might also indicate brain atrophy in the context of neurodegeneration.

3.5. Lipidomics analysis

Lipidomic analyses in plasma was performed to investigate the functional consequences of the *PCYT2*:c.4A>G variant on the lipidome. Homozygous mutant dogs showed strikingly altered lipid profiles compared to heterozygous or homozygous wildtype dogs. A significant accumulation of ether lipids, mainly of the PC-O/P class, but also of PE-O/P species, was detected in the six analyzed homozygous mutant dogs (Fig. 4).

4. Discussion

We characterized a syndromic phenotype consisting of early adult onset retinal degeneration and adult-onset neurodegenerative signs including gait abnormalities, hind limb weakness, tremors, ataxia, cognitive decline and behavioral changes such as aggression towards the owner in a group of eleven Saarlooswolfdogs (OMIA #002728–9615). A hypothesis-free genetic analysis identified a homozygous *PCYT2*:c.4A>G missense variant in all eleven affected dogs. The homozygous mutant genotype was rare in a very large cohort of clinically inconspicuous dogs. Other than in the confirmed cases, it only occurred in three relatively young dogs. We performed a detailed clinical

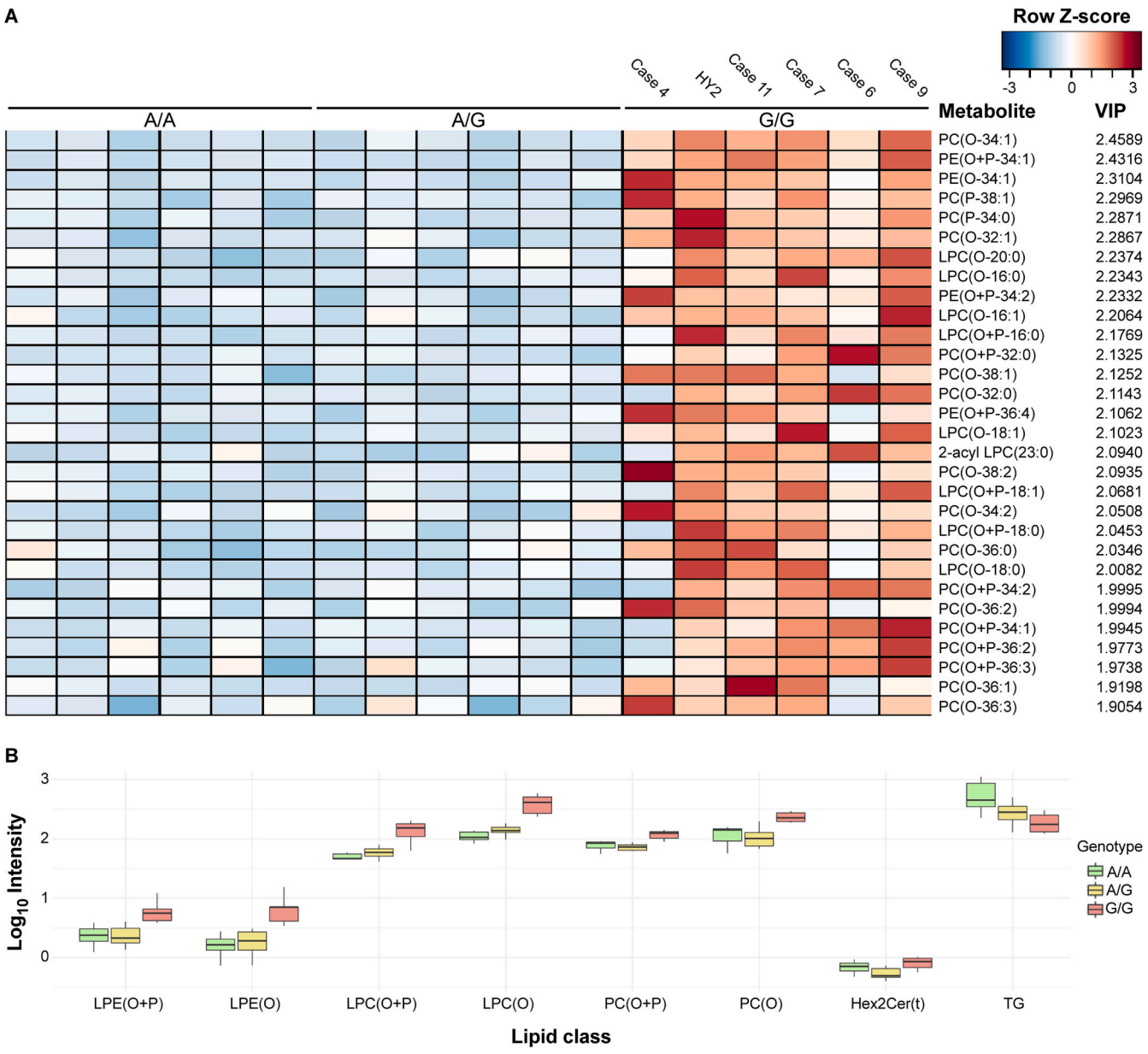

Fig. 4. Lipid profiles in plasma samples from dogs with different genotypes at *PCYT2*:c.4A>G. (A) Heatmap displaying the top 30 differential lipids ranked by Variable Importance in Projection (VIP) score in the PLS-DA model. The lipidome of the six dogs that are homozygous mutant (*G/G*) exhibits significant changes in phospholipid composition. Within brackets, 'O' denotes alkyl linkage, 'P' indicates alkenyl linkages, and 'O+P' signifies a plasmalogen structure containing both linkages, or species for which the nature of the group cannot be determined or is unknown. The numbers reflect alterations in carbon chain lengths and double bond numbers across the species.(B) Boxplots showing summation values of the 8 lipid species with significant differences between *G/G* genotype and other groups ($p \leq 0.05$ with one-way ANOVA). LPE[O+P]: Alkyl/alkenyllysophosphatidylethanolamine; LPE[O]: Alkyllysophosphatidylethanolamine; LPC[O+P]: Alkyl/alkenyllysophosphatidylcholine; LPC[O]: Alkyllysophosphatidylcholine; PC[O+P]: Alkyl/alkenylphosphatidylcholine; PC[O]: Alkylphosphatidylcholine; Hex2Cer[t]: Hydroxydihexosylceramide; TG: Triacylglycerols.

examination on one of these dogs, which revealed a beginning PRA and possible subtle changes in the brain MRI. The findings in this additional dog strongly support a pathogenic effect of the *PCYT2* variant. Furthermore, the accumulation of ether lipids in the plasma lipidome, which was exclusively seen in homozygous mutant dogs, confirmed the functional deficiency of PCYT2.

In humans, biallelic variants in *PCYT2* have been identified in patients affected with spastic paraplegia 82 (OMIM #618770) [13–18]. Age of onset and severity of clinical signs varied widely across canine and human cases alike [13–19]. Approximately half of the human patients with biallelic *PCYT2* variants became clinically evident before 1 year of age, while most dogs only were presented for ophthalmologic examination after 2 years of age.

PRA or progressive loss of vision was the only clinical feature that was reported in all eleven investigated cases, and beginning retinal degeneration was furthermore observed in the prospective investigation of HY1. Visual impairment was also a common feature in reported human cases, with 8/13 described cases suffering from loss of vision [18,19]. Interestingly, the first signs of the disease in humans were mainly gait instability and developmental delay, while blindness was the predominant first sign in dogs.

This phenotypic variability might be due to different specific effects of the different *PCYT2* variants, differences between dogs and humans, or reflect phenotypic variability often seen in inborn errors of

metabolism [31]. Studies from mice suggest that complete PCYT2 deficiency is embryonic lethal [20]. We therefore speculate that the variant reported in the dogs of our study does not completely abrogate PCYT2 function, similar to previous findings in human patients [13]. If the affected individuals retain some residual PCYT2 activity, it is conceivable that variation in other genes and/or the environment may result in different levels of PE synthesis and thus differences in the severity or age of onset of the clinical phenotype.

The histopathological investigation of case 9 revealed distinct astrocytic hypertrophy and axonal degeneration that have not yet been reported in human patients. Interestingly, PCYT2 expression is highest in astrocytes, when compared to other human brain cells [32,33]. Based on these findings, we speculate that the axonal degeneration observed in case 9 might be secondary to a defect that primarily affects astrocytes, as they are important in the homeostasis of the microenvironment around neurons, neuron support, and protection from toxic metabolites [34,35]. The pathological findings further contribute to the understanding of the pathogenesis in PCYT2 deficiency-associated neurodegeneration, potentially providing a target for further translational investigations in human patients with biallelic *PCYT2* variants.

The lipidomics changes were mostly comparable between the dogs of this study and human patients with PCYT2 deficiency [13,14,17]. It is noteworthy that these changes were also seen in dog HY2 that was clinically healthy at the time of investigation. This indicates that the altered phospholipid metabolism is the primary cause of disease. Interestingly, affected dogs not only showed increased PC, but also some elevated PE species when compared to humans [13,14,17]. This discrepancy raises the possibility of diverging PCYT2 function in dogs. Alternatively, other ways of PE synthesis might have a more dominant role in dogs compared to humans, which might also contribute to the later onset and apparently milder course of disease (young adult in dogs *vs* mostly infantile onset in humans) [13–19].

Irreversible damage to neurons and other sensitive cells occurs relatively slowly and may provide an opportunity for prophylactic intervention, if the genetic defect is diagnosed early enough. As was previously demonstrated in *Pcyt2*$^{+/-}$ mice [36], it will be interesting to see if choline substitution might restore fatty acid homeostasis and might even slow down disease progression in PCYT2 deficient dogs.

5. Conclusions

We report a homozygous *PCYT2*:c.4A>G variant as cause for PCYT2 deficiency in Saarlooswolfdogs. The studied dogs developed a syndromic phenotype comprising PRA and neurological degeneration. Our findings enable genetic testing, which can be used to avoid the unintentional breeding of further affected dogs. The studied dogs might further serve as a translational spontaneous animal model to better understand the clinical progression and possible therapeutic interventions in PCYT2 deficiency.

Supplementary data to this article can be found online at https://doi.org/10.1016/j.ymgme.2024.108149.

Funding sources

This research project was supported by a grant from the Gesellschaft zur Förderung kynologischer Forschung e.V. (GKF), private donations from the Saarlooswolfhond-Club Deutschland e.V. and a private crowdfunding initiative supporting clinical and pathological examinations. HL was supported by HiLIFE and Jane and Aatos Erkko Foundation.

CRediT authorship contribution statement

Matthias Christen: Writing – review & editing, Writing – original draft, Visualization, Investigation. **Anna Oevermann:** Writing – review & editing, Writing – original draft, Visualization, Investigation. **Stefan Rupp:** Writing – review & editing, Writing – original draft, Visualization, Investigation. **Frédéric M. Vaz:** Writing – review & editing, Writing – original draft, Visualization, Methodology, Investigation. **Eric J.M. Wever:** Writing – review & editing, Formal analysis. **Barbara K. Braus:** Writing – review & editing, Visualization, Investigation. **Vidhya Jagannathan:** Writing – review & editing, Data curation. **Alexandra Kehl:** Writing – review & editing, Resources. **Marjo K. Hytönen:** Writing – review & editing, Resources, Investigation. **Hannes Lohi:** Writing – review & editing, Resources. **Tosso Leeb:** Writing – review & editing, Writing – original draft, Supervision, Resources, Project administration, Funding acquisition, Conceptualization.

Declaration of competing interest

A.K. is an employee of Laboklin, a veterinary diagnostic laboratory that offers genetic testing for animals.

Data availability

All data are contained in this manuscript and the supplementary files. Accession numbers for the whole genome sequence data are given in Table S2.

Acknowledgements

The authors are grateful to the dog owners across Europe who donated samples and participated in the study. We especially thank the Saarlooswolfdog project team: Alexandra Windl, Sabrina Sass & Lisa van Hoof, who coordinated sample donation and phenotype collection of a big part of the samples in this study. We acknowledge the generous gift of a sample collection from the Ruhr University Bochum by Gabriele Dekomien and Jörg Epplen. Adrian Sewell provided valuable input and discussion. We thank the Next-Generation Sequencing Platform of the University of Bern for performing the high-throughput sequencing experiments and the Interfaculty Bioinformatics Unit of the University of Bern for providing high-performance computing infrastructure. We acknowledge the DBVDC consortium, the Dog10K genomes project and all researchers who deposited dog or wolf whole-genome sequencing data into public databases.

References

[1] J.E. Vance, Phospholipid synthesis and transport in mammalian cells, Traffic 16 (2015) 1–18, https://doi.org/10.1111/tra.12230.
[2] J.N. van der Veen, J.P. Kennelly, S. Wan, J.E. Vance, D.E. Vance, R.L. Jacobs, The critical role of phosphatidylcholine and phosphatidylethanolamine metabolism in health and disease, Biochim. Biophys. Acta Biomembr. 1859 (2017) 1558–1572, https://doi.org/10.1016/j.bbamem.2017.04.006.
[3] E. van den Brink-van der Laan, J.A. Killian, B. de Kruijff, Nonbilayer lipids affect peripheral and integral membrane proteins via changes in the lateral pressure profile, Biochim. Biophys. Acta 1666 (2004) 275–288, https://doi.org/10.1016/j.bbamem.2004.06.010.
[4] W. Dowhan, M. Bogdanov, Lipid-Dependent Membrane Protein Topogenesis, Annu. Rev. Biochem. 78 (2009) 515–540, https://doi.org/10.1146/annurev.biochem.77.060806.091251.
[5] E. Calzada, O. Onguka, S.M. Claypool, Phosphatidylethanolamine metabolism in health and disease, Int. Rev. Cell Mol. Biol. 321 (2016) 29–88, https://doi.org/10.1016/bs.ircmb.2015.10.001.
[6] L.F. Borkenhagen, E.P. Kennedy, L. Fielding, Enzymatic formation and decarboxylation of phosphatidylserine, J. Biol. Chem. 236 (1961), https://doi.org/10.1016/S0021-9258(19)63319-3. PC28–PC30.
[7] Y.J. Shiao, G. Lupo, J.E. Vance, Evidence that phosphatidylserine is imported into mitochondria via a mitochondria-associated membrane and that the majority of mitochondrial phosphatidylethanolamine is derived from decarboxylation of phosphatidylserine, J. Biol. Chem. 270 (1995) 11190–11198, https://doi.org/10.1074/jbc.270.19.11190.
[8] E.P. Kennedy, S.B. Weiss, The function of cytidine coenzymes in the biosynthesis of Phospholipides, J. Biol. Chem. 222 (1956) 193–214.
[9] F. Gibellini, T.K. Smith, The Kennedy pathway-De novo synthesis of phosphatidylethanolamine and phosphatidylcholine, IUBMB Life 62 (2010) 414–428, https://doi.org/10.1002/iub.337.

[10] M. Papin, A.M. Bouchet, A. Chantôme, C. Vandier, Ether-lipids and cellular signaling: a differential role of alkyl- and alkenyl-ether-lipids? Biochimie 215 (2023) 50–59, https://doi.org/10.1016/j.biochi.2023.09.004.
[11] A. Nakashima, K. Hosaka, J. Nikawa, Cloning of a human CDNA for CTP-Phosphoethanolamine Cytidylyltransferase by complementation in vivo of a yeast mutant, J. Biol. Chem. 272 (1997) 9567–9572, https://doi.org/10.1074/jbc.272.14.9567.
[12] R. Sundler, B. Akesson, Regulation of phospholipid biosynthesis in isolated rat hepatocytes. Effect of different substrates, J. Biol. Chem. 250 (1975) 3359–3367.
[13] F.M. Vaz, J.H. McDermott, M. Alders, S.B. Wortmann, S. Kölker, M.L. Pras-Raves, M.A.T. Vervaart, H. van Lenthe, A.C.M. Luyf, H.L. Elfrink, et al., Mutations in PCYT2 disrupt Etherlipid biosynthesis and cause a complex hereditary spastic paraplegia, Brain 142 (2019) 3382–3397, https://doi.org/10.1093/brain/awz291.
[14] V. Vélez-Santamaría, E. Verdura, C. Macmurdo, L. Planas-Serra, A. Schlüter, J. Casas, J.J. Martínez, C. Casasnovas, Y. Si, S.S. Thompson, et al., Expanding the clinical and genetic Spectrum of PCYT2-related disorders, Brain 143 (2020) e76, https://doi.org/10.1093/brain/awaa229.
[15] R. Kaiyrzhanov, S. Wortmann, T. Reid, M. Dehghani, M.Y. Vahidi Mehrjardi, B. Alhaddad, M. Wagner, M. Deschauer, I. Cordts, J.P. Fernandez-Murray, et al., Defective phosphatidylethanolamine biosynthesis leads to a broad Ataxia-spasticity Spectrum, Brain 144 (2021) e30, https://doi.org/10.1093/brain/awaa442.
[16] J. De Winter, D. Beijer, W. De Ridder, M. Synofzik, S.L. Zuchner, PREPARE consortium, P. Van Damme, W. Spileers, J. Baets, PCYT2 mutations disrupting Etherlipid biosynthesis: phenotypes converging on the CDP-ethanolamine pathway, Brain 144 (2021) e17, https://doi.org/10.1093/brain/awaa389.
[17] Q. Wei, W.-J. Luo, H. Yu, P.-S. Wang, H.-L. Dong, H.-F. Li, Z.-Y. Wu, A novel PCYT2 mutation identified in a Chinese consanguineous family with hereditary spastic paraplegia, J. Genet. Genom. 48 (2021) 751–754, https://doi.org/10.1016/j.jgg.2021.06.008.
[18] A.C. Mahungu, E. Steyn, N. Floudiotis, L.A. Wilson, J. Vandrovcova, M.M. Reilly, C. J. Record, M. Benatar, G. Wu, S. Raga, et al., The mutational profile in a south African cohort with inherited neuropathies and spastic paraplegia, Front. Neurol. 14 (2023) 1239725, https://doi.org/10.3389/fneur.2023.1239725.
[19] L. Leonardis, M. Skrjanec Pusenjak, A. Maver, H. Jaklic, A. Ozura Brecko, B. Koritnik, B. Peterlin, K. Writzl, Axonal polyneuropathy in 2 brothers with a homozygous missense variant in the first catalytic domain of PCYT2, Neurol. Genet 8 (2022) e658, https://doi.org/10.1212/NXG.0000000000000658.
[20] M.D. Fullerton, F. Hakimuddin, M. Bakovic, Developmental and Metabolic Effects of Disruption of the Mouse CTP:Phosphoethanolamine Cytidylyltransferase Gene (Pcyt2), Mol. Cell. Biol. 27 (2007) 3327–3336, https://doi.org/10.1128/MCB.01527-06.
[21] M.D. Fullerton, F. Hakimuddin, A. Bonen, M. Bakovic, The development of a metabolic disease phenotype in CTP:phosphoethanolamine cytidylyltransferase-deficient mice, J. Biol. Chem. 284 (2009) 25704–25713, https://doi.org/10.1074/jbc.M109.023846.
[22] D. Cikes, K. Elsayad, E. Sezgin, E. Koitai, F. Torma, M. Orthofer, R. Yarwood, L. X. Heinz, V. Sedlyarov, N.D. Miranda, et al., PCYT2-regulated lipid biosynthesis is critical to muscle health and ageing, Nat. Metab. 5 (2023) 495–515, https://doi.org/10.1038/s42255-023-00766-2.
[23] S. Purcell, B. Neale, K. Todd-Brown, L. Thomas, M.A.R. Ferreira, D. Bender, J. Maller, P. Sklar, P.I.W. de Bakker, M.J. Daly, et al., PLINK: a tool set for whole-genome association and population-based linkage analyses, Am. J. Hum. Genet. 81 (2007) 559–575, https://doi.org/10.1086/519795.
[24] G.R. Abecasis, S.S. Cherny, W.O. Cookson, L.R. Cardon, Merlin—rapid analysis of dense genetic maps using sparse gene flow trees, Nat. Genet. 30 (2002) 97–101, https://doi.org/10.1038/ng786.
[25] V. Jagannathan, C. Drögemüller, T. Leeb, G. Aguirre, C. André, D. Bannasch, D. Becker, B. Davis, K. Ekenstedt, K. Faller, et al., A comprehensive biomedical variant catalogue based on whole genome sequences of 582 dogs and eight wolves, Anim. Genet. 50 (2019) 695–704, https://doi.org/10.1111/age.12834.
[26] A. McKenna, M. Hanna, E. Banks, A. Sivachenko, K. Cibulskis, A. Kernytsky, K. Garimella, D. Altshuler, S. Gabriel, M. Daly, et al., The genome analysis toolkit: a MapReduce framework for analyzing next-generation DNA sequencing data, Genome Res. 20 (2010) 1297–1303, https://doi.org/10.1101/gr.107524.110.
[27] J.R.S. Meadows, J.M. Kidd, G.-D. Wang, H.G. Parker, P.Z. Schall, M. Bianchi, M. J. Christmas, K. Bougiouri, R.M. Buckley, C. Hitte, et al., Genome sequencing of 2000 canids by the Dog10K consortium advances the understanding of demography, Genom. Funct. Architect. Genome Biol 24 (2023) 187, https://doi.org/10.1186/s13059-023-03023-7.
[28] P. Cingolani, A. Platts, L.L. Wang, M. Coon, T. Nguyen, L. Wang, S.J. Land, X. Lu, D. M. Ruden, A program for annotating and predicting the effects of single nucleotide polymorphisms, SnpEff. Fly (Austin) 6 (2012) 80–92, https://doi.org/10.4161/fly.19695.
[29] K. Herzog, M.L. Pras-Raves, M.A.T. Vervaart, A.C.M. Luyf, A.H.C. van Kampen, R.J. A. Wanders, H.R. Waterham, F.M. Vaz, Lipidomic analysis of fibroblasts from Zellweger Spectrum disorder patients identifies disease-specific phospholipid ratios, J. Lipid Res. 57 (2016) 1447–1454, https://doi.org/10.1194/jlr.M067470.
[30] M. Molenaars, B.V. Schomakers, H.L. Elfrink, A.W. Gao, M.A.T. Vervaart, M. L. Pras-Raves, A.C. Luyf, R.L. Smith, M.G. Sterken, J.E. Kammenga, et al., Metabolomics and Lipidomics in Caenorhabditis Elegans using a single-sample preparation, Dis. Model. Mech. 14 (2021), https://doi.org/10.1242/dmm.047746.
[31] C.A. Argmann, S.M. Houten, J. Zhu, E.E. Schadt, A next generation multiscale view of inborn errors of metabolism, Cell Metab. 23 (2016) 13–26, https://doi.org/10.1016/j.cmet.2015.11.012.
[32] M. Karlsson, C. Zhang, L. Méar, W. Zhong, A. Digre, B. Katona, E. Sjöstedt, L. Butler, J. Odeberg, P. Dusart, et al., A single-cell type transcriptomics map of human tissues, Sci. Adv. 7 (2021), https://doi.org/10.1126/sciadv.abh2169.
[33] Human Protein Atlas - Single Cell Expression of PCYT2 in Human Brain, Available online: https://www.proteinatlas.org/ENSG00000185813-PCYT2/single+cell+type/brain, 2024 (accessed on 18 December 2023).
[34] G. Ricci, L. Volpi, L. Pasquali, L. Petrozzi, G. Siciliano, Astrocyte-neuron interactions in neurological disorders, J. Biol. Phys. 35 (2009) 317–336, https://doi.org/10.1007/s10867-009-9157-9.
[35] R.A. Chiareli, G.A. Carvalho, B.L. Marques, L.S. Mota, O.C. Oliveira-Lima, R. M. Gomes, A. Birbrair, R.S. Gomez, F. Simão, F. Klempin, et al., The role of astrocytes in the Neurorepair process, Front. Cell Dev. Biol. 9 (2021) 665795, https://doi.org/10.3389/fcell.2021.665795.
[36] L.C. Schenkel, S. Sivanesan, J. Zhang, B. Wuyts, A. Taylor, A. Verbrugghe, M. Bakovic, Choline supplementation restores substrate balance and alleviates complications of Pcyt2 deficiency, J. Nutr. Biochem. 26 (2015) 1221–1234, https://doi.org/10.1016/j.jnutbio.2015.05.014.